Isolating and enhancing single-photon emitters for 1550 nm quantum light sources using double nanohole optical tweezers

Zoreh Sharifi, Michael Dobinson, Ghazal Hajisalem, Mirali Seyed Shariatdoust, Adriaan L. Frencken, Frank C.J.M. van Veggel, Reuven Gordon

2021

The final publication is available at:

https://doi.org/10.1063/5.0048728

Isolating and Enhancing Single Photon Emitters for 1550 nm Quantum Light Sources using Double Nanohole Optical Tweezers

Zohreh Sharifi,[1,2] Michael Dobinson,[1,2] Ghazal Hajisalem,[1,2] Mirali Seyed Shariatdoust,[1,2] Adriaan L. Frencken,[2,3] Frank C. J. M. van Veggel,[2,3] and Reuven Gordon[1,2,a)]

[1)]*Department of Electrical and Computer Engineering, University of Victoria, Victoria, British Columbia V8P 5C2, Canada*

[2)]*Centre for Advanced Materials & Related Technologies (CAMTEC), University of Victoria, Victoria, British Columbia V8W 2Y2, Canada*

[3)]*Department of Chemistry, University of Victoria, Victoria, British Columbia V8W 2Y2, Canada*

(Dated: 20 April 2021)

Single-photons sources are required for quantum technologies and can be created from individual atoms and atom-like defects. Erbium ions produce single photons at low-loss fiber optic wavelengths, but they have low emission rates, making them challenging to isolate reliably. Here, we tune the size of gold double nanoholes (DNH) to enhance the emission of single erbium emitters, achieving 50× enhancement over rectangular apertures previously demonstrated. This produces enough enhancement to show emission from single nanocrystals at wavelengths not seen in our previous work i.e., 400 nm and 1550 nm. We observe discrete levels of emission for nanocrystals with low numbers of emitters and demonstrate isolating single emitters. We describe how the trapping time is proportional to the enhancement factor for a given DNH structure, giving us an independent way to measure the enhancement. This shows a promising path to achieving single emitter sources at 1550 nm.

I. INTRODUCTION

Single-photon sources are a key component for many quantum technologies and many efforts have explored using single atoms and atom-like defects as single emitters. Rare-earth ions have been found to be good candidates for single emitters as they produce stable emission and their quantum state can be controlled.[1–4] The need for a stable single-photon source that has high transmission efficiency in optical fibers is only increasing as quantum communication becomes more advanced.[5–7] This motivates the search for a source of single photons at low-loss telecom wavelengths for long-distance fiber propagation. Erbium is of particular interest as it emits in the C-band, the lowest-loss band for fiber transmission, a characteristic which is already widely used in erbium-doped fiber amplifiers for long-distance telecommunications.[8] Single erbium emitters have also been demonstrated, but a remaining challenge is finding a reliable method to isolate single emitters.[9]

Methods of producing single emitters typically yield random distributions and most rely on either searching among them or using low concentrations to find the single emitters.[2,10] Isolating single rare-earth emitters is particularly challenging as they have low emission rates due to long excited state lifetimes.[1] Some approaches have been explored to isolate rare-earth emitters by precisely implanting ions in crystals, making the process nearly deterministic but suffering from low yield.[11] Our group has previously demonstrated a scalable method of isolating single erbium emitters by measuring their discrete emission levels in an optical tweezer setup.[12]

Plasmonics can be used to enhance the emission rate of single emitters and make isolating them more practical. Nanoscale structures can create plasmonic enhancement which concentrates the incident electric field, enhancing emission from luminescent particles by increasing the radiative emission and non-radiative decay rates.[13–16] As applied to an Er-doped nanocrystal, this can allow a well-designed structure to increase its viability as a single photon source,[9,17] and has other applications such as photocatalysis[18] and enabling subwavelength luminescence imaging with IR excitation.[18] Structures can also be designed with multiple plasmonic resonances, which has been shown before with aperture arrays in metal.[19–21]

Plasmonic resonance not only enhances the emission, it also helps to isolate smaller particles, using the enhanced local field as optical tweezers.[22,23] Optical tweezers are well-established and have been widely used to trap and manipulate nanoparticles,[24] but trapping particles in the subwavelength scale typically requires high intensities when using conventional single beam traps. Rayleigh scattering also makes it challenging to trap and characterize small particles.[24,25] Apertures in metal films can be used to enhance the local field through plasmonic resonance, and when applied to optical tweezers this makes it easier to trap subwavelength particles well below 100 nm with lower beam intensity.[25–31] Several aperture designs have been evaluated in past works including double nanohole (DNH),[32,33] bowtie,[34,35] and rectangular[22] apertures.

Our group has previously shown that using a rectangular aperture to trap Yb–Er-doped $NaYF_4$ nanocrystals enhances emission by a factor of 400 when tuned for both the excitation and emission wavelengths.[21] Rectangular apertures have also been used by our group to trap $NaYF_4$ nanocrystals with trace doping of Er, finding discrete levels of emission. The discrete levels indicate how many emitters are present in the trapped

[a)]Corresponding author: rgordon@uvic.ca

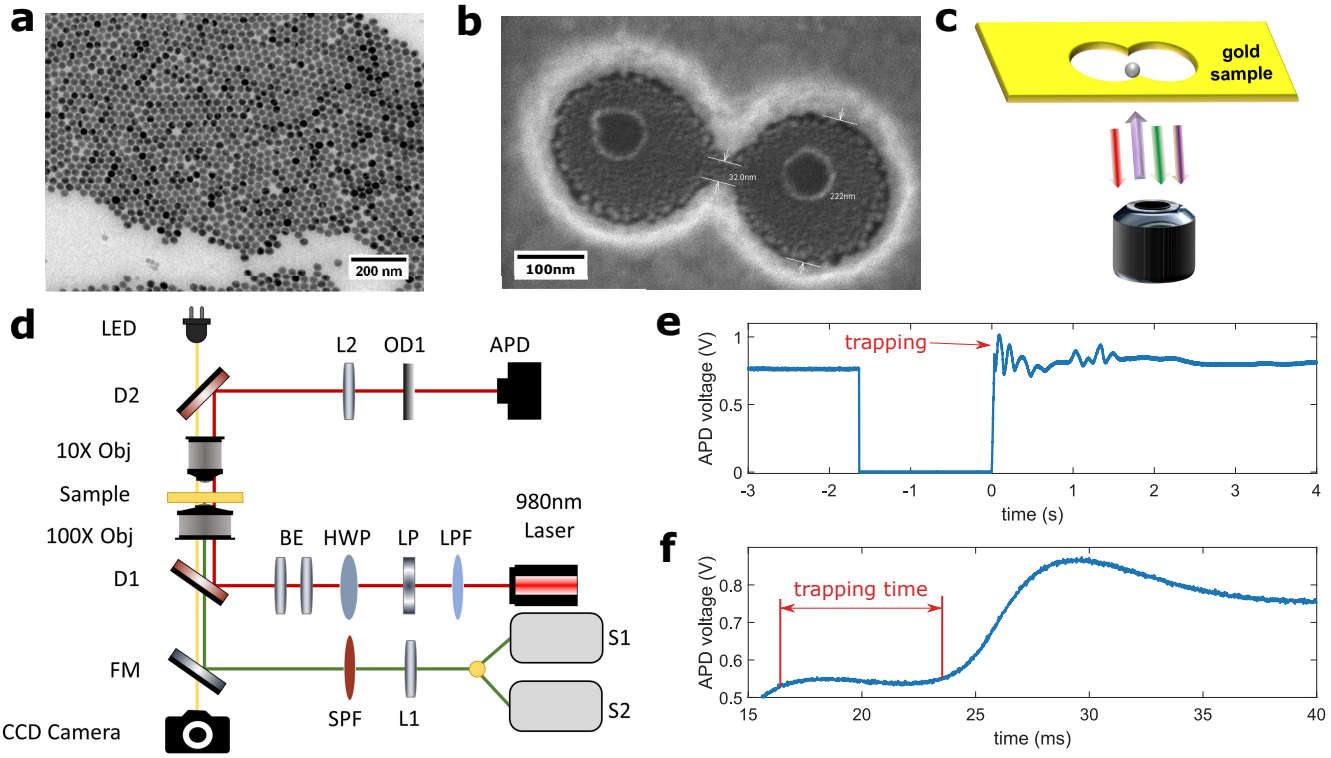

FIG. 1. Optical trapping of Yb–Er-doped $NaYF_4$ nanocrystals with DNH. (a) Image of $NaYF_4$ nanocrystals with nominal diameter of 26.2 nm. (b) Image of a fabricated DNH structure with 32 nm cusp separation and 222 nm aperture diameter, taken with scanning electron microscope. (c) Schematic of a trapped nanocrystal in a DNH aperture on a gold sample. (d) Schematic of optical tweezer setup. (e) Optical transmission through a 32 nm DNH aperture in a metal film trapping a 26.2 nm nanocrystal, as measured by the APD voltage. Laser is turned on at 0 s. (f) Magnified region showing the APD voltage change shortly after the laser is turned on and trapping time measurement.

nanocrystal, allowing nanocrystals with single emitters to be reliably isolated.[12] DNH structures have been found to produce greater local field enhancement compared to rectangular apertures, which can make isolating single emitters easier.[23] These properties make DNHs useful for other applications as well, such as biosensing.[36]

Here, we optically trap two different sizes of nanocrystals, made of $NaYF_4$ doped with 18% Yb and 2% Er, with plasmonic DNH aperture optical tweezers and characterize their emission spectra and trapping rate for different cusp separations. The DNH apertures exhibit multiple resonances within a single structure and further enhances the emission from individual nanocrystals by ~50× compared to previous findings with rectangular apertures.[21] We also, for the first time, observe new resonances from nanocrystals trapped in a DNH at 400 nm and 1550 nm.

Using the DNH apertures with the best geometry, we optically trap nanocrystals made of $NaYF_4$ with low concentrations of Er^{3+}. We observe discrete emission levels corresponding the different numbers of active emitters and isolate nanocrystals with single emitters. Furthermore, we explore the relation between the trapping dynamics and emission enhancement.

We note that recent works have used thermophoretic forces[37,38] and nanopore flow[39–41] to bring the particles closer to the surface. Since the trapping already happens in less than a second, we do not presently see any benefit for these approaches, but we do see potential of these approaches for water-based experiments where the trapping is slower (likely due to repulsive surface charges).

II. TUNING DNH APERTURE TO MAXIMIZE ENHANCEMENT

A range of DNH apertures with average cusp separations from 23 to 95 nm were fabricated to evaluate the emission enhancement. Cusp separation was the focus because the cusp is where DNH apertures produce the highest field intensity.[43,44] Samples with DNH apertures are fabricated in a 70 nm thick gold film on a glass substrate using a colloidal lithography method previously reported on by our group.[45] Scanning electron microscopy was used to measure the average cusp separation of the DNH structures in each sample. Two different sizes of nanocrystals – nominally 16.9 nm and 26.2 nm in diameter, with standard deviations of 1.3 nm and 2.7 nm – were made of $NaYF_4$ doped with 18% Yb and 2% Er, dispersed in a hexane solution. Figure 1a shows an image of the 26.2 nm nanocrystals. Figure 1b shows an example of a DNH that was fabricated with a cusp separation of 32 nm and an aperture di-

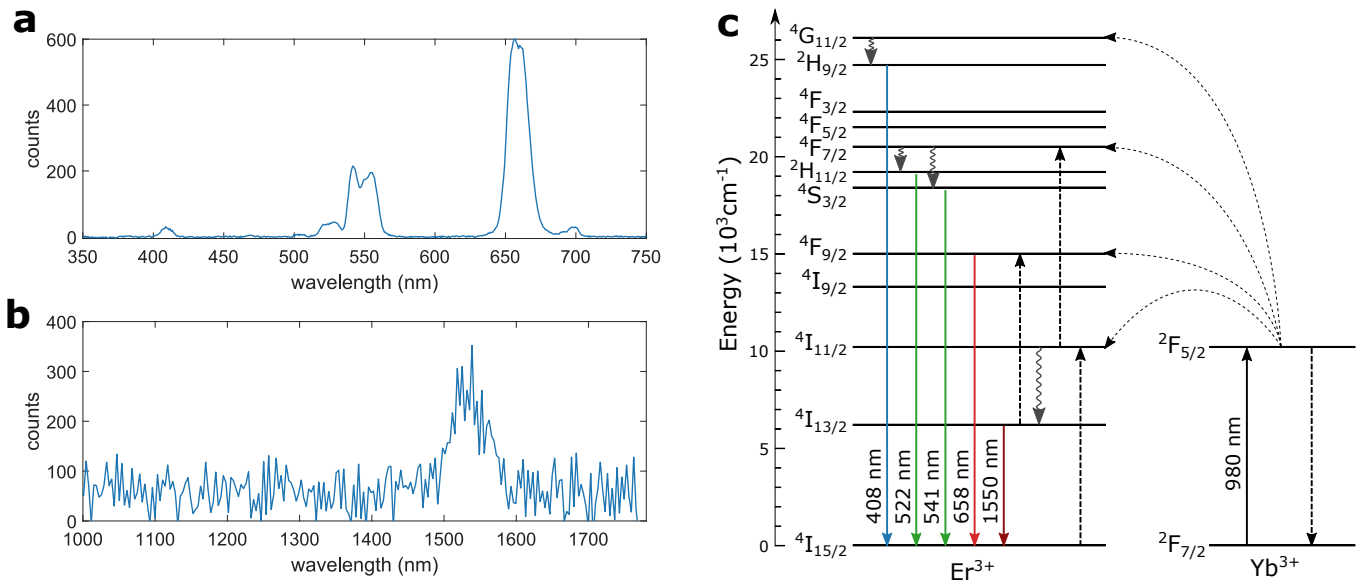

FIG. 2. Measuring the emission spectra from single nanocrystals. (a) Upconversion emission spectra from a 26.2 nm nanocrystal observed for a sample with 32 nm average cusp separation. The counts can be compared for 400, 550 and 650 nm emission peaks. Collected by a spectrometer with a 10 ms acquisition time. (b) Downconversion emission spectra from a 16.9 nm nanocrystal observed for a sample with 32 nm average cusp separation. Collected by a spectrometer with 1 s acquisition time. (c) Schematic energy level diagram of Yb^{3+} sensitizer and Er^{3+} activator in nanocrystals. Radiative energy transfer (solid lines), non-radiative energy transfer (dotted lines), cross-relaxation (dashed lines), and multiphonon relaxation (curly lines). (Adapted from Suyver et al.)[42]

ameter of 222 nm.We believe that the smaller circles are created by the nanospheres contacting the surface during deposition. Figure 1c shows a schematic of a nanocrystal trapped in a DNH aperture.

Figure 1d shows a schematic of the optical tweezer setup used to trap the nanocrystals and measure the emission spectra and trapping characteristics. A single 980 nm continuous-wave laser is used for both trapping and excitation of the nanocrystals. Trapping is confirmed by the abrupt jump in the avalanche photodiode (APD) voltage which corresponds to the transmission of light through the aperture.

Figure 1e shows the transmission of light through the DNH aperture and a representative trapping event. The laser is briefly turned off and then turned back on at 0 s. The abrupt jump in the APD voltage, compared to before the laser was turned off, confirms the trapping event.

Figure 1f shows how the trapping time is measured for the trapping event. After turning on the laser, there is a brief period (on the order of milliseconds) before a particle is trapped, this is the trapping time, t_t.

We have observed the oscillation seen in Figure 1e consistently for trapping in hexane[21], but not for trapping in water where a single step is observed[23]. We believe that it is the result of hydrodynamic interactions at the surface, in conjunction with the trapping potential; however, the detailed analysis of this effect is beyond our expertise. The oscillations are not coming from the circuit electronics.

Figures 2a and 2b show the emission of a single Yb–Er-doped $NaYF_4$ nanocrystal trapped in a DNH aperture with 32 nm average cusp separation. Emission peaks are apparent in Fig. 2a near wavelengths of 400 nm, 550 nm, and 650 nm. Figure 2b shows the emission at 1550 nm of a single Yb–Er-doped $NaYF_4$ nanocrystal trapped in a DNH aperture, which we could not observe in our previous measurements[21]. The linewidth in Figure 2b is limited by the emission band of $^4I_{13/2} \rightarrow ^4 I_{15/2}$ levels. Plasmonic resonances found in simulation are much broader. Because the 1550 nm peak is entirely the result of Er, it is not expected to vary significantly in linewidth due to the shifting plasmonic resonances with different nanoholes because the nanoholes show much broader resonances in this region of the spectrum.

We have not previously observed emissions at 400 nm and 1550 nm from single Yb–Er-doped $NaYF_4$ nanocrystals. The 400 nm upconversion emission is from the $^2H_{9/2} \rightarrow ^4 I_{15/2}$ transition in erbium.[42] The 1550 nm downconversion emission is from the $^4I_{13/2} \rightarrow ^4 I_{15/2}$ transition.[8] These transitions can be seen in the energy diagram shown in Figure 2c. Observing these two transitions from single nanocrystals for the first time in our group is possible due to the higher enhancement achieved using the double nanoholes.

Figure 3 shows the emission of the two sizes of Yb–Er-doped $NaYF_4$ nanocrystals using DNH apertures with varying average cusp separations. It illustrates how the size and shape of the aperture can impact the overall emission. Several measurements on different DNHs within each sample were taken to confirm that the measured emission is from a single trapped nanoparticle. The average of these single trapping events is taken to form the final count. The normalized standard deviation over different measurements of a single 26.2 nm nanocrystal was 2.4%, 4.3% and 6.5% and for a sin-

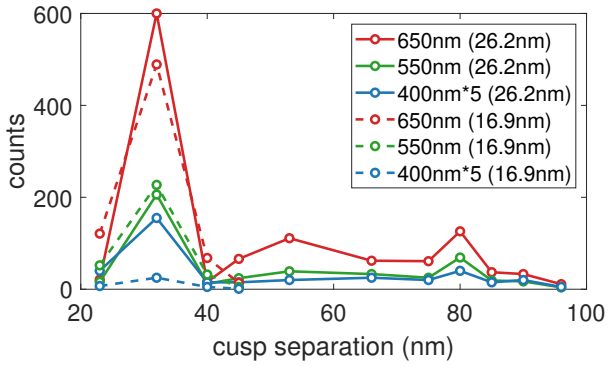

FIG. 3. Investigating the influence of the DNH cusp separation on emission enhancement. Emission from 17 nm and 26 nm nanocrystals at 400 nm, 550 nm, 650 nm for varying DNH cusp separations. Emission counts at 400 nm are multiplied by 5 for visibility.

gle 16.9 nm nanocrystal it was 3.3%, 5.6%, and 4.8%, for the 400, 550 and 650 nm emission. The laser power is maintained at ~9 mW (as measured before the 100× objective) to simultaneously excite the structure and trap the particle.

The emission and trapping characteristics of 26.2 nm Yb–Er-doped $NaYF_4$ nanocrystals are measured in ten different samples of DNH apertures with average cusp separations from 32 to 95 nm. We observe that the sample with 32 nm cusp separation has the largest emission and exhibits plasmonic resonance at additional wavelengths, 400 nm and 1550 nm, that are significantly larger than in apertures with other cusp separations. The emission was compared to previous results from our group which used the same experimental setup with rectangular apertures.[21] This aperture size showed additional enhancement factor of approximately 50, over the best rectangular aperture. With the 26.2 nm nanocrystals, enhancement at 400 nm can only be clearly seen in two samples–32 nm and 80 nm average cusp separation.

The 16.9 nm nanocrystals are used to probe the effect of smaller apertures as the 26.2 nm nanocrystals are too large to trap in DNHs with cusp separations under 32 nm. The 16.9 nm nanocrystals are too small to trap in DNHs larger than 45 nm, so the measurements for these were performed for four different samples of DNH apertures with cusp separations from 23 to 45 nm. It was seen that the 32 nm cusp size remained the peak, showing that it has optimal plasmonic resonance to enhance emission at 650 nm. There was one isolated case where a nominally 26.2 nm nanocrystal was trapped in a nominally 23 nm gap, which is possible given the size tolerances.

These results show that the resonance wavelengths shifts as the cusp separation changes. The colloidal lithography method used to prepare these samples adjusts the cusp separation by changing the plasma etching time, this also affects the diameter of the apertures. Changing both the cusp separation and aperture diameter like this can impact both the enhancement factor and resonant wavelengths.

To probe this further we look at FDTD simulations (Lumerical FDTD ver. 2020 R2.3). The simulations calculated the electric field inside the cusp of the DNH structure where the particle would be trapped as shown in Fig. 1c. The structures were modeled from SEM images similar to Fig. 1b. A total of four different DNHs were modeled around the peak of interest at 32 nm cusp separation. Figure 4a shows the simulated electric field intensity inside the cusp of a 32 nm DNH structure.

Figure 4b shows the simulation result of the relationship between the near-field electric field intensity (normalized to the incident intensity) and wavelength inside the cusp of DNH structure with different cusp separations. It can be seen that the 32 nm cusp separation has the greatest overall electric field intensity. There are two main resonant peaks for each of the simulated DNH structures. The structure with 32 nm cusp separation has peaks at 720 nm and 940 nm. The simulations were performed based on single SEM images and as the resonance frequencies are sensitive to the curvature of the cusps and the exact separation it is expected that the peaks differ slightly from the experimental results. The simulations show that multiple resonances can be used to enhance both excitation and emission wavelengths. There is minimal field enhancement seen in the simulations at 400 nm, but experimental results show increased overall emission at that wavelength. This suggests that the main effect is seen at the excitation wavelength, increasing the energy transfer, with additional resonances for other wavelengths.

III. OBSERVING DISCRETE EMISSION LEVELS

After finding that a DNH cusp separation of 32 nm shows the best enhancement with Yb-Er-doped nanocrystals, we applied this finding to search for and isolate nanocrystals with single erbium emitters. Dilute Er-doped $NaYF_4$ (with no Yb) nanocrystals were produced with a nominal diameter of 22.7 nm (standard deviation of 2.4 nm) and a nominal number of Er ions per nanocrystal of 2.48. It is expected that the Er^{3+} ions are statistically distributed within the $NaYF_4$ crystals following a Poisson distribution with $\lambda = 2.48$. As the nanocrystals have varying numbers of Er^{3+} ions, we expect to see emission counts with levels corresponding to the different number of ions that follows a similar distribution. Trapping was performed for 100 events using a DNH with 32 nm cusp separation, measuring the emission spectrum for each event.

Figure 5a shows the upconversion emission from 640 nm to 680 nm of single nanocrystals as measured with a 1 s integration time. It can be seen that the emission is separated into discrete levels. We attribute these levels to the discrete numbers of erbium emitters in the nanocrystals, from zero to seven individual active emitters. The integrated emission counts give a clear way to distinguish between the distinct numbers of active erbium emitters. The experiment demonstrated a mean of 1.68 ± 0.17 active erbium emitters per nanocrystal. Compared to the expected mean from the synthesis, this gives a yield of 0.67 ± 0.07 which is consistent with previous findings from our group.[12]

Figure 5b shows the probability distributions of Er emitters per nanocrystal as expected from the synthesis and experimental means. This distribution makes the assumption that all Er^{3+} ions can emit photons. However, it is expected that sur-

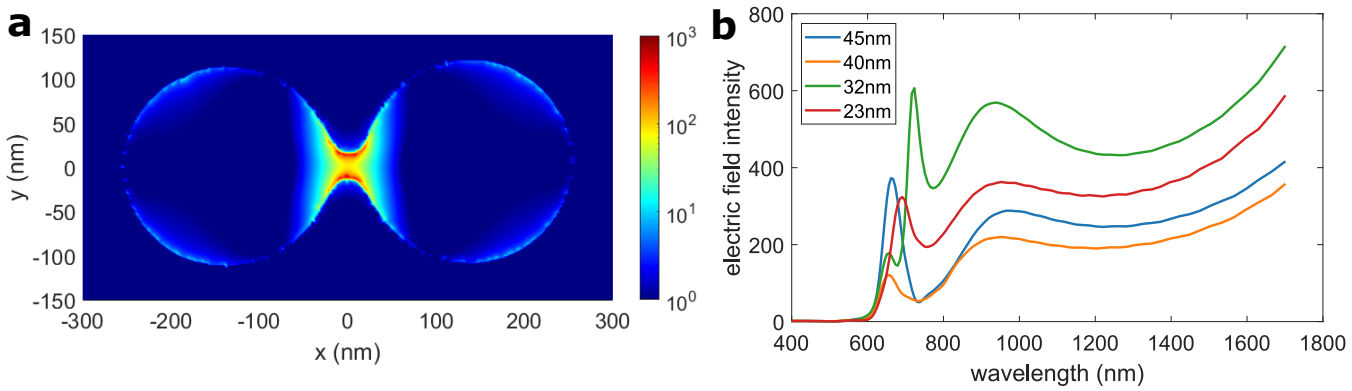

FIG. 4. Simulated electric field intensity. (a) Visualization of the electric field intensity inside of a DNH with 32 nm cusp separation. (b) Electric field intensity for DNHs with 22.7 nm, 32 nm, 40 nm, and 45 nm cusp separations. Normalized to the incident intensity.

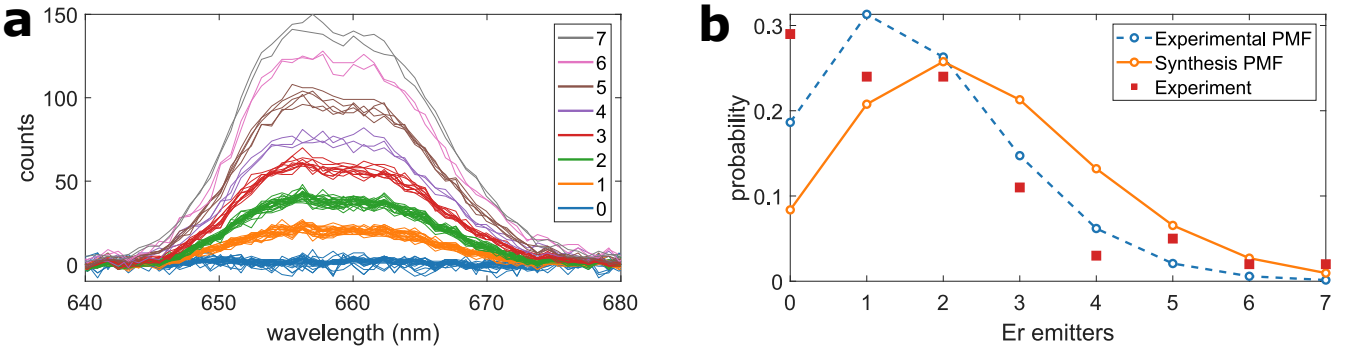

FIG. 5. Measuring discrete emission levels from low counts of erbium emitters. (a) Emission counts from nanocrystals showing discrete levels corresponding to different amounts of active erbium emitters. Collected by a spectrometer with a 1 s acquisition time. (b) Poisson probability mass functions (PMFs) for the experimental ($\lambda = 1.68$) and synthesis ($\lambda = 2.48$) and experimental probabilities for the number of Er emitters.

face quenching significantly reduces the emission from Er^{3+} ions near the surface of the nanocrystal.[46] A quenched layer of 1 nm leads to quenching of 24% of the Er^{3+} ions in the volume. This seems to be a plausible explanation considering the statistical uncertainty in the experimental results.

The different DNHs were nominally the same and therefore showed the same emission intensity. The final Poisson distribution analysis used data from several different DNHs, each following the same discrete level response.

The emission measurements were collected with a spectrometer with a 1 s acquisition time. This is an improvement by over a factor of 40 compared to previous results from our group which required a 30 s acquisition time and produced even fewer counts.[12] This is consistent with the finding in Section 2 and makes it clear that DNHs can be used to improve the process of isolating single emitters. We believe that this level of enhancement will allow for detecting and isolating single emitters at 1550 nm; however, improvements in the optical setup for that wavelength are required.

IV. TIME-TO-TRAP ANALYSIS

We also measure the trapping time from the APD voltage for the different DNH cusp separations. The analysis of the trapping time has been done previously;[32,47] here we show that the inverse of the trapping time has a similar dependence as the enhancement which we attribute to the larger trapping region with higher local field intensity.

Figure 6 shows the trapping rate (inverse of trapping time, Γ) as a function of cusp separation size. The trapping time was measured from the APD voltage (Fig. 1f) and the effect of DNH cusp separation on this factor was evaluated. With both the 16.9 nm and 26.2 nm nanocrystals, the trapping rate for the DNHs with 32 nm average cusp separation was also found to be much greater than other cusp separations. The uncertainty for the trapping time measurements was ± 2 ms. The trapping rate shown in this figure aligns closely with the emission enhancement seen in Fig. 3, with both the fastest trapping and greatest emission enhancement occurring for the 32 nm cusp separation. The 16.9 nm nanocrystals were also trapped faster on average than the 26.2 nm nanocrystals due to their smaller size and correspondingly lower Stokes' drag. In these exper-

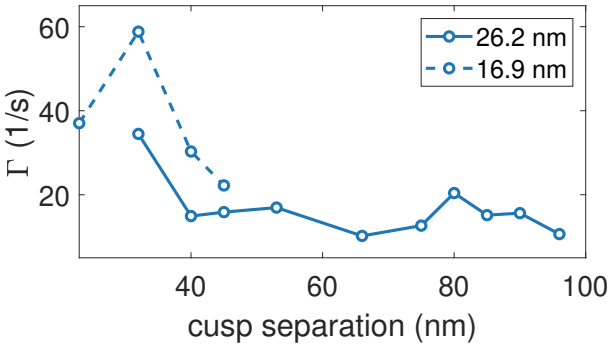

FIG. 6. Investigating the influence of the DNH cusp separation on trapping rate for 16.9 nm and 26.2 nm nanocrystals.

iments, the nanoparticle diffuses into the trapping region and the concentration of nanoparticle is maintained constant. Considering the Stokes-Einstein diffusion of 10 nm radius particles spaced by 1 micron in solution (which corresponds to the average side length of the concentration used), the expected time to reach the trap by random diffusion is 10 ms, which is the order of magnitude seen in the experiments. The concentration of the crystals was maintained the same, but the diffusion time and trapping potential size differ for different sized particles, hence 26.2 nm and 16.9 nm particles showed different times to diffuse into the trapping region.

Considering possible differences in the diffusion of nanoparticles for each aperture, multiple experiments for each sample and aperture were performed. The measurements were performed for a minimum of four DNHs in each sample and the measurements were repeated three times for each DNH.

These results demonstrate that samples with more emission enhancement also experience faster trapping, and the intensity of the emission can show how fast a particle can be pulled into trapping. While the emission enhancement and trapping dynamics are separate physical processes, they can be related to one another. It should be noted that for the enhancement seen in this experiment, it is the square of the trapping rate that is related to the emission enhancement as the emission (at 650 nm) is a two-photon process.

In the case of trapping nanocrystals, greater emission enhancement corresponds to greater intensity on the sample to excite it. Having more intensity makes the trapping region larger so the particle needs to travel less distance to get into the trap, resulting in a faster trapping time. Thermophoretic forces may also be contributing to this effect as higher local field enhancement can cause additional heating at the structure which can attract thermophilic nanoparticles to the trap.[37]

V. CONCLUSION

In conclusion, we demonstrated that the plasmonic resonances of a DNH aperture in gold film can be tuned to further enhance the emission of erbium emitters compared to rectangular apertures. The greatest enhancement for Yb–Er-doped nanocrystals was found when using DNHs with 32 nm cusp separation. The emission of single nanocrystals at 400 nm and 1550 nm was also observed for the first time. Using this finding we demonstrated isolating $NaYF_4$ nanocrystals with single active Er^{3+} emitters as determined by the discrete levels of emission. The trapping rate for varying cusp separations was measured and was found to be fastest at the same separations that produced the greatest enhancement. The increased enhancement corresponding to the higher local field intensities increases the effective size of the trap, increasing the trapping rate and giving us an independent method to measure enhancement. These results show that DNHs can be tuned to significantly enhance emission, improving the method to reliably isolate single erbium emitters. This result can be applied to isolate and measure the characteristics of single erbium emitters at 1550 nm. It is a step towards deterministically isolating single photon emitters for future single photon sources at low-loss fiber optic wavelengths. This approach can also be used for looking at other properties of lanthanide based nanoparticles such as photon avalanche at the single particle level.[48]

APPENDIX A: METHODS

Nanocrystal Synthesis and Characterization.

Chemicals. Yttrium(III) chloride hexahydrate (99.99%), erbium(III) chloride hexahydrate (99.995%), ytterbium (III) chloride hexahydrate (99.998%), ammonium fluoride (99.99%), tech grade oleic acid (90%), tech grade 1-octadecene (90%), and hexanes were purchased from Sigma-Aldrich. Anhydrous ethanol from Commercial Alcohols, methanol from Caledon, and sodium hydroxide from Bio Basic Canada inc. were used. All chemicals were used as received.

Characterization. Transmission electron microscopy images were obtained using a JEOL JEM-1400 microscope operating at 80 kV. Hexane dispersions of the NPs were drop-cast on a Formvar carbon-coated grid (300 mesh Cu) and air-dried before imaging. Size analysis of NCs from the images was performed digitally by measuring the surface area of at least 1000 particles with the program ImageJ (v. 1.52p) and calculating the corresponding diameter. X-ray diffractograms with a resolution of 0.0263 $^\circ 2\theta$ were collected using a PANalytical Empyrean X-ray System with a Cu source (Kα radiation, λ = 1.54060 Å) operating at 45 kV and 40 mA.

Synthesis (26.2 nm, $NaYF_4$: 18% Yb, 2% Er (102AF18)). To a 100 mL 3-neck roundbottom flask, 240.3 mg $YCl_3{\bullet}(H_2O)_6$, 77.8 mg $YbCl_3{\bullet}(H_2O)_6$ and 8.7 mg $ErCl_3{\bullet}(H_2O)_6$ were added together with 15 mL ODE and 5 mL oleic acid. The mixture was heated to 160 °C under vacuum and kept at that temperature for 30 minutes before cooling to room temperature. Once cooled, a solution of 107 mg NaOH and 152 mg NH_4F in 10 mL MeOH was added dropwise while stirring. The mixture was heated to 65 °C 120 minutes to evaporate the MeOH. The temperature was then raised to 298 ∘C over 20 minutes (11.75 °C/min.) Temperature was kept at 305-307 °C for 90 minutes. The mixture was then cooled, washed with 30 mL EtOH, cen-

trifuged at 1800 g for 10 min, and washed with 30 mL EtOH again before redispersion in 20 mL hexanes. TEM and XRD were performed.

Synthesis (16.9 nm $NaYF_4$: 18% Yb, 2% Er (340AF20)). To a 100 mL 3-neck roundbottom flask, 240 mg YCl_3•$(H_2O)_6$, 80 mg $YbCl_3$•$(H_2O)_6$ and 8 mg $ErCl_3$•$(H_2O)_6$ were added together with 16 mL ODE and 5 mL oleic acid. The mixture was heated to 140 °C under vacuum and kept at that temperature for 60 minutes before cooling to room temperature. Once cooled, a solution of 102 mg NaOH and 150 mg NH_4F in 10 mL MeOH was added dropwise while stirring. The mixture was heated to 70 °C 120 minutes to evaporate the MeOH. The temperature was then raised to 280 °C. Temperature was kept at 280 °C for 135 minutes. The mixture was then cooled, washed with 30 mL EtOH, centrifuged at 1800 g for 10 min, and washed with 30 mL EtOH again before redispersion in 20 mL hexanes. The sample was then centrifuged again at 8694 g for 60 minutes and the sediment was redispersed in 10 mL hexanes. TEM and XRD were performed.

Synthesis ($NaYF_4$: 2.48 Er/NP (347AF20)). To a 100 mL 3-neck roundbottom flask, 300 mg YCl_3•$(H_2O)_6$ and 0.3 mL 0.1×10^{-3} M $Er(OA)_3$ were added together with 16 mL ODE and 5 mL oleic acid. The mixture was heated to 140 °C under vacuum and kept at that temperature for 60 minutes before cooling to room temperature. Once cooled, a solution of 102 mg NaOH and 150 mg NH_4F in 10 mL MeOH was added dropwise while stirring. The mixture was heated to 70 °C 120 minutes to evaporate the MeOH. The temperature was then raised to 280 °C. Temperature was kept at 280 °C for 135 minutes. The mixture was then cooled, washed with 30 mL EtOH, centrifuged at 1800 g for 10 min, and washed with 30 mL EtOH again before redispersion in 20 mL hexanes. TEM and XRD were performed.

DNH Apertures Fabrication.

Colloidal lithography was used to fabricate double nanohole apertures. Microscope slides were cleaned using plasma for 15 minutes and sonicated for 10 minutes in an ethanol bath. 30 µL of 300 nm 0.01% w/v polystyrene spheres in ethanol drop-coated on the microscope slides uniformly. While the solution dries out through evaporation, the polystyrene spheres attach to the slides. The prepared slides were plasma etched with 5 to 15 seconds difference in etching time to get different cusp separation on each sample. Using 5 nm of titanium as an adhesive layer followed by 70 nm of gold, the samples were sputtered (MANTIS Sputtering System). The sputtered samples were sonicated for 1 minute in a toluene bath to remove polystyrene beads. SEM was performed.

Optical Trapping.

The optical tweezer setup (Fig. 1d) consists of a single 980 nm continuous-wave laser (JDS Uniphase SDLO-27-7552-160-LD) which is collimated, filtered, polarized, and expanded, before being focused on the sample with a 100× oil immersion microscope objective (1.25 numerical aperture). This single beam is used for both trapping, and to excite the nanocrystals. A 10× microscope objective is used to collect the light transmitted through the sample which is measured by an avalanche photodetector (Thorlabs APD120A). The polarization of the beam is set by the half-wave plate (HWP) and the linear polarizer (LP). A three-axis sample stage with piezoelectric adjustment aligns the apertures to the beam with 20 nm precision. A 750 nm short-pass filter (Thorlabs FES0750) reduces the trapping beam intensity and a bifurcated fiber splits the signal between two spectrometers, one for visible wavelengths (Ocean Optics QE65000) and one for NIR wavelengths (BaySpec NIRS-0900-1700). The gold DNH aperture samples were attached to #0 coverslips with an adhesive spacer containing 17.6 µL of nanocrystals in hexane with concentrations of 1.3×10^{12} nanoparticles/cm^3, 5×10^{12} nanoparticles/cm^3, and 4×10^{12} nanoparticles/cm^3 for the 16.9 nm, 22.7 nm, and 26.2 nm nanocrystals.

Abbreviations used in Figure 1d: APD, avalanche photodetector; BE, beam expander; CCD, charge-coupled device; D, dichroic mirrror; FM, flip mirror; HWP, half-wave plate; LP, linear polarizer; LPF, long-pass filter; Obj, objective lens; OD, optical density filter; S, spectrometer; SPF, short-pass filter.

AUTHOR CONTRIBUTIONS

Z.Sh. and M.D. performed the trapping experiments. Z.Sh. analyzed the data. A.L.F. and F.C.J.M.v.V. were responsible for nanocrystal synthesis and characterization. M.S.S. performed the FDTD simulations. R.G. conceived the experiment. All authors assisted in writing the manuscript.

Disclosures. The authors declare no conflicts of interest.

ACKNOWLEDGMENTS

The authors acknowledge funding support from the NSERC Discovery Grants program RGPIN-2017-03830 and RGPIN-2018-03743.

DATA AVAILABILITY

The data that support the findings of this study are available from the corresponding author upon reasonable request.

REFERENCES

[1] G. Liu and B. Jacquier, eds., *Spectroscopic Properties of Rare Earths in Optical Materials*, Springer Series in Materials Science (Springer-Verlag, Berlin Heidelberg, 2005).

[2] R. Kolesov, K. Xia, R. Reuter, R. Stöhr, A. Zappe, J. Meijer, P. Hemmer, and J. Wrachtrup, "Optical detection of a single rare-earth ion in a crystal," Nature Communications **3**, 1029 (2012).

[3] R. Kolesov, K. Xia, R. Reuter, M. Jamali, R. Stöhr, T. Inal, P. Siyushev, and J. Wrachtrup, "Mapping Spin Coherence of a Single Rare-Earth Ion in a Crystal onto a Single Photon Polarization State," Physical Review Letters **111**, 120502 (2013).

[4] K. Xia, R. Kolesov, Y. Wang, P. Siyushev, R. Reuter, T. Kornher, N. Kukharchyk, A. D. Wieck, B. Villa, S. Yang, and J. Wrachtrup, "All-Optical Preparation of Coherent Dark States of a Single Rare Earth Ion Spin in a Crystal," Physical Review Letters **115**, 093602 (2015).

[5]N. Gisin, "How far can one send a photon?" Frontiers of Physics **10**, 100307 (2015).
[6]M. D. Eisaman, J. Fan, A. Migdall, and S. V. Polyakov, "Invited Review Article: Single-photon sources and detectors," Review of Scientific Instruments **82**, 071101 (2011).
[7]Y.-A. Chen, Q. Zhang, T.-Y. Chen, W.-Q. Cai, S.-K. Liao, J. Zhang, K. Chen, J. Yin, J.-G. Ren, Z. Chen, S.-L. Han, Q. Yu, K. Liang, F. Zhou, X. Yuan, M.-S. Zhao, T.-Y. Wang, X. Jiang, L. Zhang, W.-Y. Liu, Y. Li, Q. Shen, Y. Cao, C.-Y. Lu, R. Shu, J.-Y. Wang, L. Li, N.-L. Liu, F. Xu, X.-B. Wang, C.-Z. Peng, and J.-W. Pan, "An integrated space-to-ground quantum communication network over 4,600 kilometres," Nature , 1–6 (2021).
[8]E. Desurvire, *Erbium-Doped Fiber Amplifiers: Principles and Applications*, Vol. 48 (1995).
[9]A. M. Dibos, M. Raha, C. M. Phenicie, and J. D. Thompson, "Atomic Source of Single Photons in the Telecom Band," Physical Review Letters **120**, 243601 (2018).
[10]W. Redjem, A. Durand, T. Herzig, A. Benali, S. Pezzagna, J. Meijer, A. Y. Kuznetsov, H. S. Nguyen, S. Cueff, J.-M. Gérard, I. Robert-Philip, B. Gil, D. Caliste, P. Pochet, M. Abbarchi, V. Jacques, A. Dréau, and G. Cassabois, "Single artificial atoms in silicon emitting at telecom wavelengths," Nature Electronics **3**, 738–743 (2020).
[11]K. Groot-Berning, T. Kornher, G. Jacob, F. Stopp, S. T. Dawkins, R. Kolesov, J. Wrachtrup, K. Singer, and F. Schmidt-Kaler, "Deterministic Single-Ion Implantation of Rare-Earth Ions for Nanometer-Resolution Color-Center Generation," Physical Review Letters **123**, 106802 (2019).
[12]A. Alizadehkhaledi, A. L. Frencken, F. C. J. M. van Veggel, and R. Gordon, "Isolating Nanocrystals with an Individual Erbium Emitter: A Route to a Stable Single-Photon Source at 1550 nm Wavelength," Nano Letters **20**, 1018–1022 (2020).
[13]P. J. Schuck, D. P. Fromm, A. Sundaramurthy, G. S. Kino, and W. E. Moerner, "Improving the Mismatch between Light and Nanoscale Objects with Gold Bowtie Nanoantennas," Physical Review Letters **94**, 017402 (2005).
[14]S. A. Maier, *Plasmonics: Fundamentals and Applications* (Springer, New York, 2007).
[15]D. M. Wu, A. García-Etxarri, A. Salleo, and J. A. Dionne, "Plasmon-Enhanced Upconversion," The Journal of Physical Chemistry Letters **5**, 4020–4031 (2014).
[16]A. Teitelboim, B. Tian, D. J. Garfield, A. Fernandez-Bravo, A. C. Gotlin, P. J. Schuck, B. E. Cohen, and E. M. Chan, "Energy Transfer Networks within Upconverting Nanoparticles Are Complex Systems with Collective, Robust, and History-Dependent Dynamics," The Journal of Physical Chemistry C **123**, 2678–2689 (2019).
[17]T. Zhong, J. M. Kindem, J. G. Bartholomew, J. Rochman, I. Craiciu, V. Verma, S. W. Nam, F. Marsili, M. D. Shaw, A. D. Beyer, and A. Faraon, "Optically Addressing Single Rare-Earth Ions in a Nanophotonic Cavity," Physical Review Letters **121**, 183603 (2018).
[18]B. Zhou, B. Shi, D. Jin, and X. Liu, "Controlling upconversion nanocrystals for emerging applications," Nature Nanotechnology **10**, 924–936 (2015).
[19]M. Saboktakin, X. Ye, U. K. Chettiar, N. Engheta, C. B. Murray, and C. R. Kagan, "Plasmonic Enhancement of Nanophosphor Upconversion Luminescence in Au Nanohole Arrays," ACS Nano **7**, 7186–7192 (2013).
[20]E. Verhagen, L. Kuipers, and A. Polman, "Field enhancement in metallic subwavelength aperture arrays probed by erbium upconversion luminescence," Optics Express **17**, 14586–14598 (2009).
[21]A. Alizadehkhaledi, A. L. Frencken, M. K. Dezfouli, S. Hughes, F. C. J. M. van Veggel, and R. Gordon, "Cascaded Plasmon-Enhanced Emission from a Single Upconverting Nanocrystal," ACS Photonics **6**, 1125–1131 (2019).
[22]C. Chen, M. L. Juan, Y. Li, G. Maes, G. Borghs, P. Van Dorpe, and R. Quidant, "Enhanced Optical Trapping and Arrangement of Nano-Objects in a Plasmonic Nanocavity," Nano Letters **12**, 125–132 (2011).
[23]Y. Pang and R. Gordon, "Optical Trapping of 12 nm Dielectric Spheres Using Double-Nanoholes in a Gold Film," Nano Letters **11**, 3763–3767 (2011).
[24]A. Ashkin, J. M. Dziedzic, J. E. Bjorkholm, and S. Chu, "Observation of a single-beam gradient force optical trap for dielectric particles," Optics Letters **11**, 288–290 (1986).
[25]E.-S. Kwak, T.-D. Onuta, D. Amarie, R. Potyrailo, B. Stein, S. C. Jacobson, W. L. Schaich, and B. Dragnea, "Optical Trapping with Integrated Near-Field Apertures," The Journal of Physical Chemistry B **108**, 13607–13612 (2004).
[26]K. Okamoto and S. Kawata, "Radiation Force Exerted on Subwavelength Particles near a Nanoaperture," Physical Review Letters **83**, 4534–4537 (1999).
[27]M. L. Juan, R. Gordon, Y. Pang, F. Eftekhari, and R. Quidant, "Self-induced back-action optical trapping of dielectric nanoparticles," Nature Physics **5**, 915–919 (2009).
[28]B. J. Roxworthy, K. D. Ko, A. Kumar, K. H. Fung, E. K. C. Chow, G. L. Liu, N. X. Fang, and K. C. Toussaint, "Application of Plasmonic Bowtie Nanoantenna Arrays for Optical Trapping, Stacking, and Sorting," Nano Letters **12**, 796–801 (2012).
[29]M. Righini, A. S. Zelenina, C. Girard, and R. Quidant, "Parallel and selective trapping in a patterned plasmonic landscape," Nature Physics **3**, 477–480 (2007).
[30]M. Righini, G. Volpe, C. Girard, D. Petrov, and R. Quidant, "Surface Plasmon Optical Tweezers: Tunable Optical Manipulation in the Femtonewton Range," Physical Review Letters **100**, 186804 (2008).
[31]M. Righini, P. Ghenuche, S. Cherukulappurath, V. Myroshnychenko, F. J. García de Abajo, and R. Quidant, "Nano-optical Trapping of Rayleigh Particles and Escherichia coli Bacteria with Resonant Optical Antennas," Nano Letters **9**, 3387–3391 (2009).
[32]A. Kotnala and R. Gordon, "Quantification of High-Efficiency Trapping of Nanoparticles in a Double Nanohole Optical Tweezer," Nano Letters **14**, 853–856 (2014).
[33]H. Xu, S. Jones, B.-C. Choi, and R. Gordon, "Characterization of Individual Magnetic Nanoparticles in Solution by Double Nanohole Optical Tweezers," Nano Letters **16**, 2639–2643 (2016).
[34]R. A. Jensen, I.-C. Huang, O. Chen, J. T. Choy, T. S. Bischof, M. Lončar, and M. G. Bawendi, "Optical Trapping and Two-Photon Excitation of Colloidal Quantum Dots Using Bowtie Apertures," ACS Photonics **3**, 423–427 (2016).
[35]J. Berthelot, S. S. Aćimović, M. L. Juan, M. P. Kreuzer, J. Renger, and R. Quidant, "Three-dimensional manipulation with scanning near-field optical nanotweezers," Nature Nanotechnology **9**, 295–299 (2014).
[36]M. U. Raza, S. S. S. Peri, L.-C. Ma, S. M. Iqbal, and G. Alexandrakis, "Self-induced back action actuated nanopore electrophoresis (SANE)," Nanotechnology **29**, 435501 (2018).
[37]Q. Jiang, B. Rogez, J.-B. Claude, G. Baffou, and J. Wenger, "Quantifying the Role of the Surfactant and the Thermophoretic Force in Plasmonic Nano-optical Trapping," Nano Letters **20**, 8811–8817 (2020).
[38]C. Hong, S. Yang, and J. C. Ndukaife, "Stand-off trapping and manipulation of sub-10 nm objects and biomolecules using opto-thermo-electrohydrodynamic tweezers," Nature Nanotechnology **15**, 908–913 (2020).
[39]S. S. S. Peri, M. K. Sabnani, M. U. Raza, E. L. Urquhart, S. Ghaffari, J. S. Lee, M. J. Kim, J. Weidanz, and G. Alexandrakis, "Quantification of low affinity binding interactions between natural killer cell inhibitory receptors and targeting ligands with a self-induced back-action actuated nanopore electrophoresis (sane) sensor," Nanotechnology **32**, 045501 (2020).
[40]D. Verschueren, X. Shi, and C. Dekker, "Nano-Optical Tweezing of Single Proteins in Plasmonic Nanopores," Small Methods **3**, 1800465 (2019).
[41]F. Eftekhari, C. Escobedo, J. Ferreira, X. Duan, E. M. Girotto, A. G. Brolo, R. Gordon, and D. Sinton, "Nanoholes as nanochannels: flow-through plasmonic sensing," Analytical chemistry **81**, 4308–4311 (2009).
[42]J. F. Suyver, J. Grimm, M. K. van Veen, D. Biner, K. W. Krämer, and H. U. Güdel, "Upconversion spectroscopy and properties of NaYF4 doped with Er3+, Tm3+ and/or Yb3+," Journal of Luminescence **117**, 1–12 (2006).
[43]A. Lesuffleur, L. K. S. Kumar, and R. Gordon, "Enhanced second harmonic generation from nanoscale double-hole arrays in a gold film," Applied Physics Letters **88**, 261104 (2006).
[44]A. Lesuffleur, L. K. S. Kumar, A. G. Brolo, K. L. Kavanagh, and R. Gordon, "Apex-Enhanced Raman Spectroscopy Using Double-Hole Arrays in a Gold Film," The Journal of Physical Chemistry C **111**, 2347–2350 (2007).
[45]A. L. Ravindranath, M. S. Shariatdoust, S. Mathew, and R. Gordon, "Colloidal lithography double-nanohole optical trapping of nanoparticles and proteins," Optics Express **27**, 16184 (2019).
[46]F. Wang, J. Wang, and X. Liu, "Direct Evidence of a Surface Quenching Effect on Size-Dependent Luminescence of Upconversion Nanoparticles," Angewandte Chemie International Edition **49**, 7456–7460 (2010).
[47]A. Kotnala, D. DePaoli, and R. Gordon, "Sensing nanoparticles using a double nanohole optical trap," Lab on a Chip **13**, 4142–4146 (2013).

[48]C. Lee, E. Z. Xu, Y. Liu, A. Teitelboim, K. Yao, A. Fernandez-Bravo, A. M. Kotulska, S. H. Nam, Y. D. Suh, A. Bednarkiewicz, B. E. Cohen, E. M. Chan, and P. J. Schuck, "Giant nonlinear optical responses from photon-avalanching nanoparticles," Nature **589**, 230–235 (2021).